fermentation

MDPI

Article

Enhancing Freezing Stress Tolerance through Regulation of the Ubiquitin–Proteasome System in *Saccharomyces cerevisiae*

Ryoya Tanahashi [1,2,†], Akira Nishimura [1,*,†], Kyoyuki Kan [3], Natsumi Ishizaki [4], Shiho Fujishima [4], Hisanori Endo [4] and Hiroshi Takagi [1,*]

[1] Institute for Research Initiatives, Nara Institute of Science and Technology, 8916-5 Takayama-cho, Ikoma 630-0192, Nara, Japan
[2] Department of Food Science and Technology, University of California Davis, One Shields Ave., Davis, CA 95616, USA
[3] Division of Biological Science, Graduate School of Science and Technology, Nara Institute of Science and Technology, 8916-5 Takayama-cho, Ikoma 630-0192, Nara, Japan
[4] Food R&D Center, TableMark Co., Ltd., Ota 144-0042, Tokyo, Japan
* Correspondence: nishimura@bs.naist.jp (A.N.); hiro@bs.naist.jp (H.T.); Tel.: +81-743-72-6207 (A.N.); +81-743-72-5601 (H.T.)
† These authors contribute equally to this work.

Abstract: The baking industry is experiencing significant growth, primarily due to the widespread adoption of frozen dough baking. However, this process can negatively impact the fermentation ability of yeast, as freezing can induce stress in yeast cells. This study reports the molecular interplay between the ubiquitin–proteasome system and freezing stress tolerance in the yeast *Saccharomyces cerevisiae*. Using the proteasome inhibitor MG132, we first screened mutants with enhanced freezing stress tolerance. Three mutants showed elevated activity of the intracellular proteasome, particularly trypsin-like activity (more than threefold) and reduced sensitivity to MG132 inhibition of chymotrypsin-like activity (less than 0.125-fold). Genomic analysis of these mutants revealed mutations in the *ROX1* gene, a heme-dependent repressor of hypoxic genes. Importantly, the *ROX1* deletion strain displayed slightly improved freezing stress tolerance (about 1.5-fold). Comprehensive transcription analysis identified the *ANB1* gene as a potential downstream target of Rox1. Overexpression of *ANB1* enhanced freezing stress tolerance (about 1.5-fold) with increased the proteasome's activity, indicating that Rox1 contributes to changes in the proteasome's activity and freezing stress tolerance through the function of Anb1. The present data provide new insights into the mechanisms of freezing stress tolerance and help us improve the baking of frozen dough to produce higher-quality bread.

Keywords: *Saccharomyces cerevisiae*; ubiquitin–proteasome system; frozen dough baking

check for updates

Citation: Tanahashi, R.; Nishimura, A.; Kan, K.; Ishizaki, N.; Fujishima, S.; Endo, H.; Takagi, H. Enhancing Freezing Stress Tolerance through Regulation of the Ubiquitin–Proteasome System in *Saccharomyces cerevisiae*. *Fermentation* **2024**, *10*, 318. https://doi.org/10.3390/fermentation10060318

Academic Editor: Ogueri Nwaiwu

Received: 18 April 2024
Revised: 7 June 2024
Accepted: 15 June 2024
Published: 17 June 2024

Copyright: © 2024 by the authors. Licensee MDPI, Basel, Switzerland. This article is an open access article distributed under the terms and conditions of the Creative Commons Attribution (CC BY) license (https://creativecommons.org/licenses/by/4.0/).

1. Introduction

The baking industry has been expanding, with the market size reaching about US$220 billion in the fiscal year of 2022 (TableMark Co., Ltd., Tokyo, Japan, personal communication). The fastest growing segment in the industry currently is frozen dough baking, a method whereby frozen dough is thawed, fermented, and baked in quantities determined by the sales conditions. This trend is driven by consumers' desire for convenience and to enjoy freshly baked products that can be easily prepared by pulling them out of the freezer. However, the freezing process can induce stress on yeast cells in dough, which negatively impacts fermentation [1,2].

The baker's yeast *Saccharomyces cerevisiae* (*S. cerevisiae*) produces ethanol and CO_2 in dough during fermentation. Ethanol gives dough its distinct flavor, while CO_2 increases its volume. Unfortunately, the frozen dough baking method often leads to insufficient dough expansion and lack of flavor, resulting in a decrease in the quality of the final product.

Therefore, yeast strains with advanced freezing stress tolerance would be promising for use in frozen dough baking.

Freezing stress (stress caused by freezing and thawing) occurs when intracellular water grows into ice crystals, causing damage to biomolecules. Yeast cells possess inherent mechanisms to respond and adapt to many environmental stresses. Under freezing stress conditions, yeast cells exhibit various responses to maintain cellular homeostasis, including the expression of low-temperature chaperones [3], the accumulation of compatible solutes such as trehalose [4], and changes in the cell membrane's composition involving unsaturated fatty acids [5]. The intracellular trehalose and glycerol could be important in protecting yeast cells from the formation of ice crystals. Additionally, extracellular amino acids such as proline have cryoprotective activity. Furthermore, under freezing stress conditions, the generation of reactive oxygen species (ROS) due to mitochondrial damage has been reported [6,7]. Both ice crystals and ROS cause severe damage to intracellular proteins. In other words, the freezing process is a proteotoxic stress. Therefore, post-freezing yeast exhibits an accumulation of denatured proteins, leading to significant reductions in viability and fermentation ability. A recent study has revealed a link between the ubiquitin–proteasome system, which is responsible for clearing denatured proteins, and tolerance to freezing stress, suggesting the possibility of new breeding strategies [8].

Protein quality control mechanisms consist of two systems: the degradation system mediated by ubiquitin and proteasome, and the repair system involving chaperones. Chaperones can refold misfolded proteins into their native conformation but are ineffective against severe protein misfolding (denaturation). Freezing stress can cause severe protein damage, and the degradation system may be the primary mechanism for the quality control of protein under freezing stress. In the ubiquitin–proteasome system, denatured proteins are recognized and ubiquitinated by ubiquitin ligases associated with the protein-related quality control mechanism [9–11]. Denatured proteins tagged with polyubiquitin chains are then transported to the 26S proteasome complex for degradation and removal [12,13]. The proteasome's function includes caspase-like, trypsin-like, and chymotrypsin-like activities, each exhibiting substrate specificity and participating cooperatively in the degradation of denatured proteins.

The 26S proteasome complex consists of two subunits: the regulatory particle (19S RP) and the core particle (CP or 20S proteasome) [11,13,14]. The 19S RP recognizes polyubiquitin chains, unfolds the substrate's proteins, and transports them into the CP [15–17]. The CP acts as the catalytic subunit of the proteasome, forming a barrel-shaped structure by stacking α1–α7 and β1–β7 in an αββα sequence. Among the β subunits, β1 (encoded by the *PRE3* gene) is involved in caspase-like activity, β2 (encoded by the *PUP1* gene) in trypsin-like activity, and β5 (encoded by the *PRE2* gene) in chymotrypsin-like activity. Peptide-based proteasome inhibitors such as MG132 can bind to the catalytic sites of the β subunits (β1, β2, and β5), inhibiting the proteasome's activity [18].

Both transcriptional and post-translational mechanisms regulate the 26S proteasome [11]. Many structural genes of the proteasome are positively regulated by the transcription factor Rpn4, resulting in a marked reduction in the amount of 26S proteasome in the *RPN4*-deficient strain [19,20]. The *RPN4* gene controls proteasome levels in response to various stresses. Rpn4 is ubiquitinated by the ubiquitin ligase Ubr2 and rapidly degraded by the 26S proteasome [21]. Thus, deletion of *UBR2* results in the accumulation of the 26S proteasome. The post-translational regulation of the 26S proteasome involves pathways associated with Fub1 and chaperones. Fub1 was identified as an endogenous proteasome inhibitory protein in vitro but as an activator in vivo. Moreover, the assembly of the 26S proteasome is controlled by a number of molecular chaperones, with Pba1–Pba4 and Ump1 involved in the assembly of α rings and β rings, respectively [22–24]. Furthermore, the N-terminal region of Pre2 (β5), which is responsible for chymotrypsin-like activity, is a molecular chaperone known as β5pro and is essential for assembling the 26S proteasome [25–27]. However, the role of β5pro is still unclear. Currently, the mechanisms and functions of

post-translational regulation of the 26S proteasome are less comprehensively understood than those of the transcriptional control.

Yeast cells use compatible solutes to tolerate freezing stress by preventing the formation of intracellular ice crystals. The addition of these compounds to the culture medium and optimization of the culture conditions can increase the amount of compatible solutes inside the cells, making them more tolerant to freezing stress. However, the addition of such solutes can raise production costs and may alter the taste, flavor, and texture of the bread, which may not be acceptable to both producers and consumers. An alternative approach to obtaining strains with numerous qualities is breeding. Breeding strategies that use metabolic engineering to target specific cellular systems have less impact on other systems that affect the bread's taste and aroma. Furthermore, the generated strains can be distributed worldwide, allowing people to make high-quality bread without changing their traditional bread-making methods. Therefore, breeding strategies with metabolic engineering have advantages in obtaining practical candidates with improved freezing stress capabilities.

Frozen dough baking has many advantages over conventional baking methods. However, cells of baker's yeast are exposed to severe freezing stress, which limits their fermentation ability. Although the proteasome system has been well studied, the molecular relationship between the proteasome system and freezing stress tolerance has not been fully understood. In this study, we investigated the relationship between the ubiquitin–proteasome system and freezing stress tolerance in *S. cerevisiae*. Screening with MG132 identified mutants with enhanced freezing stress tolerance, characterized by increased intracellular proteasome activity, particularly trypsin-like proteasome activity, and by decreased sensitivity to MG132 inhibition of chymotrypsin-like activity. Whole-genome sequencing showed that loss-of-function mutations in *ROX1*, a heme-dependent repressor of hypoxic genes, result in enhanced freezing stress tolerance. Therefore, transcription analysis revealed *ANB1* as a potential downstream target gene of Rox1. These findings provided insight into the mechanisms of tolerance to freezing stress and their potential applications in developing baker's yeast strains.

2. Materials and Methods

2.1. Culture Medium

The growth media used in this study were a yeast extract, peptone, and dextrose medium (YPD) (1% yeast extract (Difco Laboratories, Detroit, MI, USA), 2% peptone (Difco Laboratories), and 2% glucose), a synthetic complete medium (SC) (2% glucose, 0.5% ammonium sulfate, 0.17% yeast nitrogen base without amino acids and ammonium sulfate (Difco Laboratories), 0.008% proline, 0.04% leucine, 0.008% alanine, 0.008% asparagine, 0.008% aspartic acid, 0.008% glutamine, 0.008% glutamic acid, 0.008% cysteine, 0.008% glycine, 0.008% histidine, 0.008% isoleucine, 0.008% lysine, 0.008% methionine, 0.008% phenylalanine, 0.008% serine, 0.008% threonine, 0.008% tryptophane, 0.008% valine, 0.008% uracil, 0.008% inositol, 0.008% p-aminobenzoic acid, and 0.002% adenine), a synthetic complete medium without uracil (SC-Ura) (SC medium without uracil), and a model dough medium (6.57% glucose, 0.57% urea, 0.57% ammonium sulfate, 0.23% magnesium sulfate, 0.00045% thiamine hydrochloride, 0.00045% pyridoxine hydrochloride, 0.0045% nicotinic acid, and 67 mM potassium phosphate; pH 6.0). SC and SC-Ura were adjusted to pH 6.5 with NaOH. When necessary, 2% agar (Nacalai Tesque, Kyoto, Japan) was added to solidify the medium. All media were sterilized at 121 °C for 20 min.

2.2. Strains

Tables S1 and S2 summarize the yeast strains and oligonucleotide primers used in this study. The *rpn4*Δ and *ubr2*Δ strains were constructed from a wild-type (WT) strain by integrating the *kanMX6* gene cassette amplified by PCR with gene-specific primer sets (RPN4 dis fw and RPN4 dis rv for the *RPN4* deletion, UBR2 dis fw and UBR2 dis rv for the *UBR2* deletion; Table S2) and pFA6a-kanMX6 (purchased from the AddGene repository).

For the construction of the *erg6*Δ strain, an *ERG6* gene-specific deletion cassette containing the *bleMX6* gene that was amplified by PCR with the primers ERG6 dis fw and ERG6 dis rv (Table S2) and pFA6-bleMX6 (purchased from the AddGene repository), was integrated into the genome of the WT strain. To construct the *erg6*Δ*pdr5*Δ strain, a *PDR5* gene-specific deletion cassette containing the *kanMX6* gene, amplified by PCR with the primers PDR5 dis fw and PDR5 dis rv (Table S2) and pFA6-kanMX6, was integrated into the genome of the *erg6*Δ strain. The *erg6*Δ*pdr5*Δ*rox1*Δ and *rox1*Δ strains were constructed by inserting a *ROX1* gene-specific deletion cassette containing the *natNT2* gene, amplified by PCR with the primers ROX1 dis fw and ROX1 dis rv (Table S2) and the plasmid pFA6-natNT2 (purchased from the AddGene repository), into the genome of the *erg6*Δ*pdr5*Δ and WT strains. For the construction of the *erg6*Δ*pdr5*Δ*ura3*Δ and *ura3*Δ strains, a *URA3* gene-specific deletion cassette containing the *hphNT1* gene, amplified by PCR with the primers URA3 dis fw and URA3 dis rv (Table S2) and the plasmid pFA6-hphNT1 (purchased from the AddGene repository), was inserted into the genome of the *erg6*Δ*pdr5*Δ and WT strains. The *rox1*Δ*anb1*Δ and *anb1*Δ strains were constructed by inserting an *ANB1* gene-specific deletion cassette containing the *hphNT1* gene, amplified by PCR with the primers ANB1 dis fw and ANB1 dis rv (Table S2) and the plasmid pFA6-hphNT1 (purchased from the AddGene repository), into the genome of the *rox1*Δ and WT strains.

2.3. Plasmids

The plasmids pAG416-P_{GPD}-*ANB1*, -*YPR064W*, -*HEM13*, -*SUR2*, -*DIA3*, -*LAC1*, -*ROG3*, -*YPR015C*, -*GID10*, -*FRD1*, -*MHF1*, -*YAR029W*, and -*HYP2* were constructed using a gateway technology (Thermo Fisher Scientific, Waltham, MA, USA) following the manufacturer's instructions. ORFs were obtained from the plasmids BG1805-*ANB1*, -*YPR064W*, -*HEM13*, -*SUR2*, -*DIA3*, -*LAC1*, -*ROG3*, -*YPR015C*, -*GID10*, -*FRD1*, -*MHF1*, -*YAR029W*, and -*HYP2* (Horizon Discovery, Cambridge, UK). The plasmid pAG416-P_{GPD}-ccdB-HA was used as the gateway destination vector. The *anb1*^{K51R} mutant gene was constructed using a QuikChange II XL Site-Directed Mutagenesis Kit (Agilent, Santa Clara, CA, USA) and the mutagenic primer pair ANB1-K51R fw and ANB1-K51R rv.

2.4. Cell Viability

Yeast strains precultured in SC or SC-Ura medium were suspended in distilled water to an optical density at 600 nm (OD_{600}) of 1.0. The suspensions were stored at −30 °C for the time points indicated in the figure legends. After thawing at 25 °C for 20 min, the cells were diluted 1000-fold with distilled water and spread onto YPD. Colonies were counted after incubation at 30 °C for 3 days to determine cell viability. Cell viability was calculated as follows: (numbers of colonies after freezing stress treatment/numbers of colonies before freezing stress treatment) × 100.

2.5. Growth Test

Yeast cells were cultured at 30 °C in SC medium starting at an OD_{600} of 0.1 under shaking conditions. The cells' growth was monitored by measuring OD_{600} with a DU-800 spectrophotometer (Beckman Coulter, Brea, CA, USA).

2.6. Fermentation of the Model Dough

Yeast strains were cultured in 50 mL of SC or SC-Ura medium until reaching the stationary phase (30 °C, 200 rpm), and cells with an OD_{600} were collected in units of 20. The cells were then washed with distilled water, suspended in distilled water, and incubated at −30 °C for 5 days. After thawing at 25 °C for 20 min, the cells were suspended in 25 mL of the model dough medium. The fermentation process was continuously monitored by measuring the volume of evolved CO_2 gas using a Fermograph II apparatus (ATTO Technology Inc., Amherst, NY, USA) under static incubation conditions at 30 °C.

2.7. Spot Test

After yeast cells were diluted to an OD_{600} of 1.0 with water, aliquots of 10-fold serial dilutions were spotted onto YPD plates containing 50 μM MG132. The plates were incubated at 30 °C for 3 days.

2.8. Isolation of Mutants Resistant to MG132

The strain *erg6*Δ*pdr5*Δ was grown at 30 °C in YPD medium to the stationary phase. After the cells had been washed twice with distilled water, 10^7 cells were plated on YPD medium supplemented with 50 μM MG132. After incubation at 30 °C for 3 days, colonies were picked and named MT1-19.

2.9. Whole-Genome Sequencing

MT3, -4, and -10 were grown in YPD medium at 30 °C for 2 days with shaking. The cells were then harvested, washed twice with distilled water, and suspended in phenol/chloroform. Genomic DNA was extracted using a multi-bead shocker (MB601U; Yasui Kikai, Osaka, Japan) with 0.5 mm glass beads and was purified by ethanol precipitation. Libraries for sequencing analysis were prepared using an NEB Next Ultra DNA Library Prep Kit (New England Biolabs, Ipswich, MA, USA), and paired-end short reads of 150 bp were produced using an Illumina NovaSeq 6000 system (Illumina Inc., San Diego, CA, USA). A quality control process was applied to the raw paired-end sequence reads that passed the FastQC stage. Low-quality (<20) bases and adapter sequences were trimmed by Trimmomatic software (version 0.38), and a final coverage of 96–98% was obtained. The reads were mapped to the *S. cerevisiae* S288C reference genome (version R64-1-1) with Bwa-mem (v0.7.17-r1188), using the default parameters. The number of duplicates was calculated using Picard MarkDuplicates, and single-nucleotide variants (SNVs) and short indels were called using Bcftools (Version 1.9). To identify the putative effects on protein translation and high-impact mutations, the identified variants were annotated using SnpEff (Version 4.3t). The sequencing processes were conducted by a commercial DNA sequencing service (Rhelixa Inc., Tokyo, Japan).

2.10. Activity of the Proteasome

Yeast strains were grown in SC or SC-Ura medium to the stationary phase. The cells were harvested, suspended with an extraction buffer (50 mM phosphate buffer, 1 mM $MgCl_2$, pH 7.0), and disrupted using a multi-bead shocker with 0.5-mm glass beads. The supernatant (crude enzyme) was obtained by centrifugation at 15,000 rpm for 20 min. The proteasome's activity was assayed by measuring the fluorescence of 7-amino-4-methylcoumarin (AMC) generated after the enzymatic reaction (250 μg/mL of crude enzyme with 100 μM of each fluorescent substrate). The intensity of fluorescence was detected using a TriStar LB942 instrument (Berthold Technologies, Bad Wildbad, Germany) with an excitation wavelength of 355 nm and an emission wavelength of 460 nm. The fluorescent substrates were Ac-RLR-AMC (Cayman Chemical, Ann Arbor, MI, USA) for trypsin-like activity, Suc-LLVY-MCA (Peptide Institute, Osaka, Japan) for chymotrypsin-like activity, and Z-LLE-MCA (Peptide Institute) for caspase-like activity. MG132 was used at a final concentration of 50 μM to assess the sensitivity of the strains to MG132 inhibition. The numerical values in the figures represent the percentage of residual activity in the presence of MG132. It was calculated by dividing the activity with MG132 by the activity without MG132.

2.11. Determination of COX5b and ANB1 mRNA

Yeast cells were cultured in SC medium at 30 °C to the stationary phase and were disrupted using the multi-bead shocker with 0.5 mm glass beads. Following the manufacturer's instructions, the total RNA was extracted with a NucleoSpin RNA plus kit (Takara Bio, Shiga, Japan). The cDNA was synthesized from total RNA using a PrimeScript RT reagent kit (Takara Bio). The relative abundance of *COX5b* and *ANB1* mRNAs was quanti-

fied by quantitative PCR (qPCR) using a QuantStudio3 system (Thermo Fisher Scientific) and SsoAdvanced Universal SYBR Green Supermix (Bio-Rad Laboratories, Hercules, CA, USA). The following primer sets (listed in Table S2) were used in this analysis: COX5b qPCR fw and COX5b qPCR rv (PCR efficiency: 96.1%), and ANB1 qPCR fw and ANB1 qPCR rv (PCR efficiency: 92.4%). The following PCR protocol was used: 95 °C for 4 min, followed by 40 cycles of denaturation at 95 °C for 15 s and annealing/extension at 60 °C for 30 s. The cycle threshold of each gene was normalized to that of the housekeeping gene *ACT1*, and the relative expression levels were calculated using the $2^{-\Delta\Delta Ct}$ method.

2.12. RNAseq Analysis

Yeast strains were precultured in SC medium at 30 °C to the stationary phase. The cells were then washed twice with distilled water and resuspended in distilled water to a concentration of OD_{600} = 100. The suspension was stored at −30 °C for 5 days. After thawing for 20 or 40 min at 25 °C, cells were disrupted using the multi-bead shocker with 0.5 mm glass beads. The total RNA was extracted using a NucleoSpin RNA Plus kit following the manufacturer's instructions. A quality control process was applied to the raw paired-end sequence reads that passed the FastQC. Low-quality (<20) bases and adapter sequences were trimmed by Trimmomatic software (Version 0.38). Reads were aligned to the *S. cerevisiae* reference genome (version R64-1-1) using the RNA-seq aligner HISAT2 (Version 2.1.0). The coverage was 96–98%. The matrix of expression counts was generated using featureCounts (Version 1.6.3). The raw read counts were normalized as transcripts per million (TPM). A commercial service performed the RNAseq analysis (Rhelixa Inc.).

2.13. Statistical Analysis

Data are presented as the means ± standard deviation (SD), and statistical significance was evaluated using Student's *t*-test and one-way/two-way analysis of variance (ANOVA) with Tukey's test. These analyses were performed using Prism 7 (GraphPad Software, San Diego, CA, USA). Values of $p < 0.05$ were considered statistically significant.

3. Results

The proteasome's activity relates to freezing stress tolerance in yeast.

To confirm that freezing stress reduces yeast's fermentation, we measured the cells' viability and total CO_2 emissions after freezing (Figure S1). Total CO_2 emissions are an indicator of the fermentation ability of yeast cells. The data showed that freezing stress significantly decreased both the cells' viability and yeast's fermentation ability. Next, we constructed the *RPN4*- or *UBR2*-deleted strain (*rpn4*Δ or *ubr2*Δ) to investigate whether the proteasome's activity contributes to freezing stress tolerance. It is known that *rpn4*Δ suppresses the expression of proteasome-related genes, resulting in reduced activity of the proteasome [28]. Meanwhile, deletion of *UBR2* stabilizes the Rpn4 protein, thereby increasing the proteasome's activity [28]. There was no significant difference in growth among the WT, *rpn4*Δ, and *ubr2*Δ strains (Figure S2A). Compared with the WT, *rpn4*Δ was more sensitive to freezing stress, while *ubr2*Δ showed increased tolerance (Figure S2B). These data indicated that the ubiquitin–proteasome system is related to freezing stress tolerance.

Given the potential of activation of the proteasome to increase freezing stress tolerance, we performed a screen using the proteasome inhibitor MG132 (Figure 1A). MG132 generally has little effect on WT cells because it cannot penetrate the yeast cells' membrane. Deletion of the *ERG6* gene in the ergosterol biosynthetic pathway has been reported to cause an increase in drug permeability [29]. Deleting the *PDR5* gene encoding a multidrug transporter reduced drug efflux from cells [30]. Therefore, we generated strains sensitive to MG132 by constructing a double deletion mutant (*erg6*Δ*pdr5*Δ) of the *ERG6* and *PDR5* genes. Figure 1B indicates that *erg6*Δ*pdr5*Δ showed dramatically greater sensitivity to MG132 compared with the WT and *erg6*Δ (Figure 1B). From the genetic screen with MG132 and *erg6*Δ*pdr5*Δ, we obtained 19 spontaneous mutants (hereafter referred to as MT strains)

that were able to grow on the MG132-containing medium, unlike *erg6*Δ*pdr5*Δ (Figure 1C). Rough comparisons suggested that the MT strains grew slightly more slowly than the WT strain (Figure 1B,C). The freezing stress tolerance of the MT strains was then examined, and 16 strains exhibited a higher survival rate after freezing stress than *erg6*Δ*pdr5*Δ (Figure 1D).

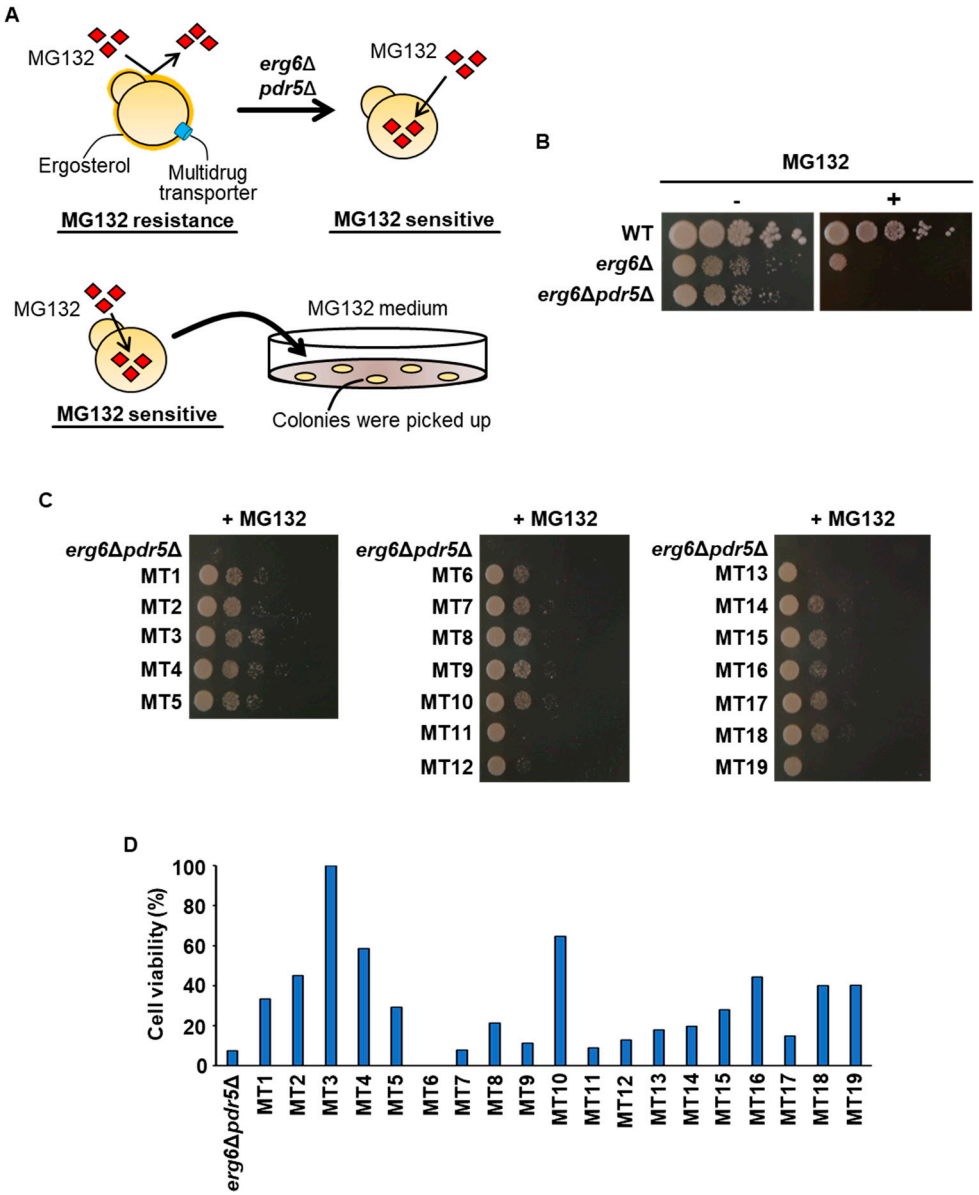


Figure 1. Screening of MG132-resistant strains. (**A**) Schematic representation of the screening in this study. The upper panel illustrates the construction of an MG132-sensitive strain. Due to ergosterol and multidrug transporters, MG132 cannot be accumulated in yeast cells. To increase MG132 toxicity, the *ERG6* gene in the ergosterol biosynthetic pathway and the *PDR5* gene encoding a multidrug transporter were disrupted. The lower panel shows the screening of spontaneous mutants growing on the medium supplemented with MG132. The MG132-sensitive *erg6*Δ*pdr5*Δ strain cannot grow on the medium containing MG132. However, when mutations occur in the genes involved in inhibition of the proteasome's activity by MG132, yeast cells can grow on the MG132-supplemented medium. The positions of the mutations were identified by whole-genome sequencing. (**B**) Effects of *ERG6* and *PDR5* deletion on sensitivity to MG132. WT, *erg6*Δ, and *erg6*Δ*pdr5*Δ cells were spotted onto YPD medium without/with 50 μM MG132. (**C**) Growth on the MG132-supplemented medium. The MG132-sensitive *erg6*Δ*pdr5*Δ and MT mutants obtained via the screening process were spotted onto

YPD medium with 50 μM MG132. (**D**) The cell's viability after freezing stress. The strain *erg6*Δ*pdr5*Δ and MT mutants obtained in the screening were stored at −30 °C for 5 days. After thawing at 25 °C for 20 min, the cells were spread onto YPD plates, and the cells' viability was determined by measuring the colony-forming units. The data represent a single experiment (n = 1).

Among these mutants, MT3, MT4, and MT10 exhibited particularly high freezing stress tolerance. Therefore, we performed a reproducibility test to confirm the freezing stress tolerance of these three mutants (Figure 2A). As shown in Figure 2A, MT3, MT4, and MT10 exhibited significantly higher survival after freezing stress compared with *erg6*Δ*pdr5*Δ. To determine the possibility of enhanced proteasome activity in these strains, we measured the proteasome's activity (trypsin-like, chymotrypsin-like, and caspase-like activity) using fluorescent substrates for each protease (Figure 2B–D). Trypsin-like activity was significantly higher in each of MT3, MT4, and MT10 than in *erg6*Δ*pdr5*Δ, whereas chymotrypsin-like activity was markedly lower in *erg6*Δ*pdr5*Δ. There was no significant difference in caspase-like activity between *erg6*Δ*pdr5*Δ and MT3, MT4, or MT10. We then examined the inhibitory effects of MG132 on the proteasome's activity (Figure 2B–D). There was no significant difference between *erg6*Δ*pdr5*Δ and MT3, MT4, or MT10 in the sensitivity to MG132-based inhibition of trypsin-like and caspase-like activities. Importantly, the sensitivity to MG132-based inhibition of chymotrypsin-like activity was lower in MT3, MT4, and MT10 compared with *erg6*Δ*pdr5*Δ. Thus, changes in the proteasome's activity and MG132 sensitivity may contribute to the improved freezing stress and MG132 resistance of MT3, MT4, and MT10.

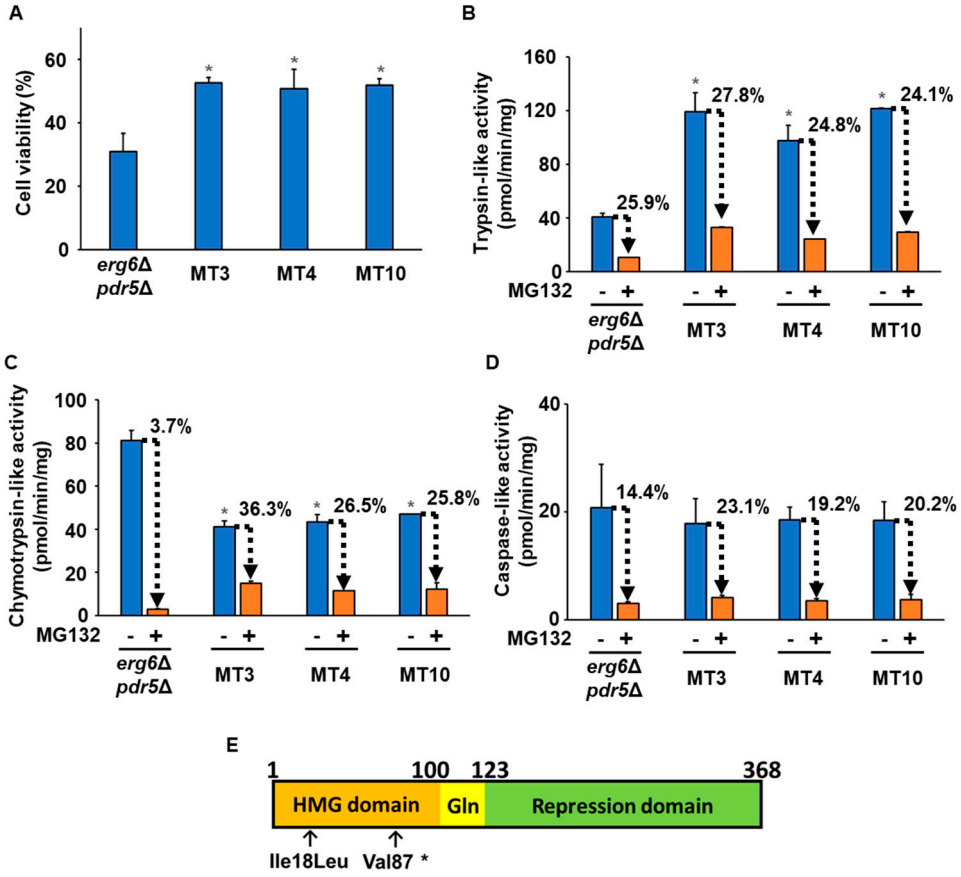


Figure 2. *Cont.*

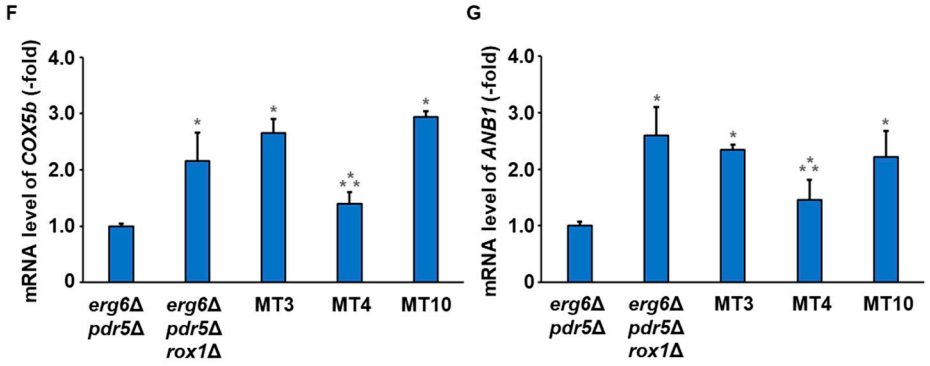


Figure 2. Characterization of MT mutants. (**A**) The cells' viability after freezing stress. The MG132-sensitive *erg6*Δ*pdr5*Δ, MT3, MT4, and MT10 strains were stored at −30 °C for 5 days. After thawing at 25 °C for 20 min, the cells were spread onto YPD plates, and the cells' viability was determined by measuring the colony-forming units. Data are presented as the means ± SD (n = 3), and statistical significance was determined by Student's t-test. * $p < 0.05$ vs. *erg6*Δ*pdr5*Δ. (**B**) Trypsin-like activity. Trypsin-like activity in *erg6*Δ*pdr5*Δ, MT3, MT4, and MT10 was determined by the fluorescence of AMC generated from Ac-RLR-AMC during the enzymatic reaction without/with 50 μM MG132. Data are presented as the means ± SD (n = 3), and statistical significance was determined by Student's t-test. * $p < 0.05$ vs. *erg6*Δ*pdr5*Δ -MG132. (**C**) Chymotrypsin-like activity. Chymotrypsin-like activity in *erg6*Δ*pdr5*Δ, MT3, MT4, and MT10 was determined by the fluorescence of AMC generated from Suc-LLVY-MCA during the enzymatic reaction without/with 50 μM MG132. Data are presented as the means ± SD (n = 3), and statistical significance was determined by Student's t-test. * $p < 0.05$ vs. *erg6*Δ*pdr5*Δ -MG132. (**D**) Caspase-like activity. Caspase-like activity in *erg6*Δ*pdr5*Δ, MT3, MT4, and MT10 was determined by the fluorescence of AMC generated from Z-LLE-MCA during the enzymatic reaction without/with 50 μM MG132. Data are presented as the means ± SD (n = 3), and statistical significance was determined by Student's t-test. (**E**) Schematic representation of the domain structures within Rox1. HMG domain, DNA-binding domain; Repression domain, transcriptional regulatory domain; Gln, glutamine-rich motif (unknown function). The arrows indicate the sites of an amino acid change (Ile18Leu and Val87*) in the HMG domain. (**F**) Expression levels of the *COX1b* gene. The mRNA levels of *COX1b* in *erg6*Δ*pdr5*Δ, MT3, MT4, and MT10 were determined by qPCR. Data are presented as the means ± SD (n = 3), and statistical significance was determined by one-way ANOVA with Tukey's test. * $p < 0.05$ vs. *erg6*Δ*pdr5*Δ; ** $p < 0.05$ vs. *erg6*Δ*pdr5*Δ*rox1*Δ. (**G**) Expression levels of the *ANB1* gene. The mRNA levels of *ANB1* in *erg6*Δ*pdr5*Δ, MT3, MT4, and MT10 were determined by qPCR. Data are presented as the means ± SD (n = 3), and statistical significance was determined by one-way ANOVA with Tukey's test. * $p < 0.05$ vs. *erg6*Δ*pdr5*Δ; ** $p < 0.05$ vs. *erg6*Δ*pdr5*Δ*rox1*Δ.

To identify mutations involved in the altered activity of the proteasome and improved freezing stress tolerance in MT3, MT4, and MT10, whole-genome sequencing analysis was performed for these strains. The search for DNA mutations causing amino acid substitutions in the genome of each mutant revealed mutations in the *ROX1* (Regulation by OXygen) gene in all mutants (Table 1). Rox1 is a transcriptional repressor of low-oxygen-responsive genes (e.g., *COX5b* and *ANB1*). Therefore, *ROX1*-deficient strains express low-oxygen-responsive genes even in the presence of oxygen [31]. Mutations that cause a complete deletion of the transcriptional regulatory domain of Rox1 were identified in MT3 and MT10, suggesting that MT3 and MT10 have a loss-of-function mutation of Rox1 (Figure 2E). In contrast, MT4 carried a mutation with an amino acid substitution (Ile18Leu) within the DNA binding domain (HMG domain) of Rox1. We then measured the transcription levels of low-oxygen-responsive genes (*COX5b* and *ANB1*) by qPCR. Figure 2F,G show that the transcription levels of *COX5b* and *ANB1* in MT3 and MT10 were almost the same as those in the *ROX1*-deficient strain (*erg6*Δ*pdr5*Δ*rox1*Δ). The transcription levels of *COX5b* and *ANB1* in MT4 were significantly higher than in *erg6*Δ*pdr5*Δ but lower than in *erg6*Δ*pdr5*Δ*rox1*Δ. These results suggested that the Rox1 variant (Val87*) in MT3 and

MT10 is a loss-of-function mutation, whereas the Rox1 variant (Ile18Leu) in MT4 exhibited reduced function. Therefore, the reduced function of Rox1 may be responsible for the changes in the proteasome's activity and the improvements in freezing stress tolerance in MT3, MT4, and MT10.

Table 1. List of mutations identified in the genomes of the three mutants.

Strain	Gene	Mutation (DNA)	Substitution (Amino acid)
MT3	*ROX1*	257 del C	Pro 86 Arg, Val 87 Stop
MT4	*ROX1*	52 A > C	Ile18 Leu Stop
MT10	*ROX1*	257 del C	Pro 86 Arg, Val 87 Stop

ROX1 deletion confers freezing stress tolerance on yeast cells by modulating the proteasome's activity.

Next, we characterized the *ROX1*-deleted strains. Figure 3A indicates that the *ROX1* knockout strain (*erg6*Δ*pdr5*Δ*rox1*Δ) exhibited increased resistance to MG132 compared with *erg6*Δ*pdr5*Δ, similar to MT3, MT4, and MT10. Analysis of the proteasome's activity in *erg6*Δ*pdr5*Δ*rox1*Δ showed increased trypsin-like activity but decreased chymotrypsin-like activity compared with *erg6*Δ*pdr5*Δ (Figure 3B,C). In addition, both strains showed a comparable level of caspase-like activity (Figure 3D). Observation of the MG132 sensitivity of the proteasome's activities revealed no significant difference in the sensitivity of trypsin-like or caspase-like activities between the two strains. However, *erg6*Δ*pdr5*Δ*rox1*Δ showed a decrease in the MG132 sensitivity of chymotrypsin-like activity (Figure 3C). Furthermore, the freezing stress tolerance of *erg6*Δ*pdr5*Δ*rox1*Δ was significantly higher than that of *erg6*Δ*pdr5*Δ (Figure 3E). These data were consistent with the observed characteristics of MT3, MT4, and MT10, suggesting that loss of the function of Rox1 was responsible for the altered activity of the proteasome and enhanced freezing stress tolerance in MT3, MT4, and MT10.

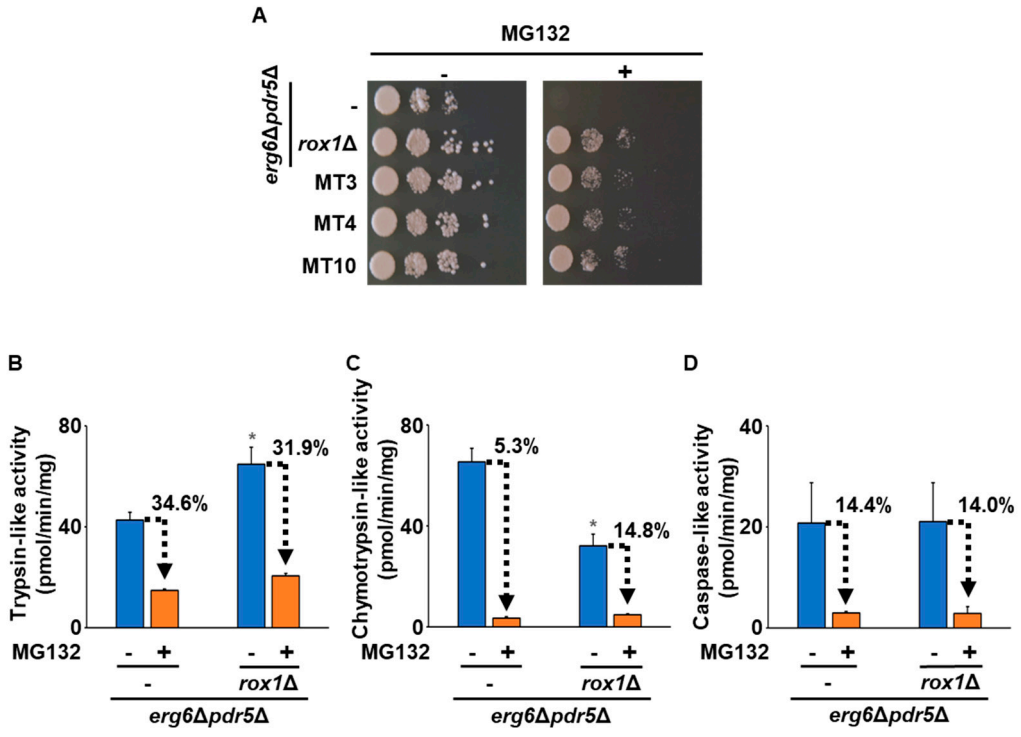


Figure 3. *Cont.*

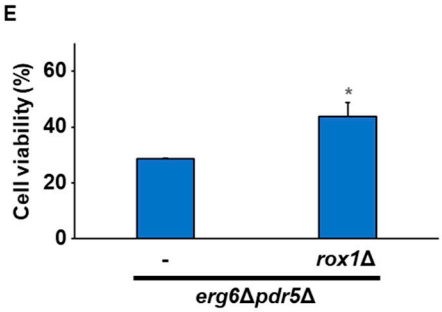


Figure 3. Effects of the deletion of *ROX1* on the proteasome's activity and freezing stress tolerance. (**A**) Growth on the MG132-supplemented medium. The strains *erg6*Δ*pdr5*Δ, *erg6*Δ*pdr5*Δ*rox1*Δ, MT3, MT4, and MT10 were spotted onto YPD plates without/with 50 μM MG132. (**B**) Trypsin-like activity. Trypsin-like activity in *erg6*Δ*pdr5*Δ and *erg6*Δ*pdr5*Δ*rox1*Δ was determined by the fluorescence of AMC generated from Ac-RLR-AMC during the enzymatic reaction without/with 50 μM MG132. Data are presented as the means ± SD (n = 3), and statistical significance was determined by Student's t-test. * $p < 0.05$ vs. *erg6*Δ*pdr5*Δ -MG132. (**C**) Chymotrypsin-like activity. Chymotrypsin-like activity in *erg6*Δ*pdr5*Δ and *erg6*Δ*pdr5*Δ*rox1*Δ was determined by the fluorescence of AMC generated from Suc-LLVY-MCA during the enzymatic reaction without/with 50 μM MG132. Data are presented as the means ± SD (n = 3), and statistical significance was determined by Student's t-test. * $p < 0.05$ vs. *erg6*Δ*pdr5*Δ-MG132. (**D**) Caspase-like activity. Caspase-like activity in *erg6*Δ*pdr5*Δ and *erg6*Δ*pdr5*Δ*rox1*Δ was determined by the fluorescence of AMC generated from Z-LLE-MCA during the enzymatic reaction without/with 50 μM MG132. Data are presented as the means ± SD (n = 3), and statistical significance was determined by Student's t-test. (**E**) The cells' viability after freezing stress. The *erg6*Δ*pdr5*Δ and *erg6*Δ*pdr5*Δ*rox1*Δ strains were stored at −30 °C for 5 days. After thawing at 25 °C for 20 min, the cells were spread onto YPD plates, and the cells' viability was determined by measuring the colony-forming units. Data are presented as the means ± SD (n = 3), and statistical significance was determined by Student's t-test. * $p < 0.05$ vs. *erg6*Δ*pdr5*Δ.

We next constructed a *ROX1* knockout (*rox1*Δ) strain from the WT strain and examined its characteristics. Measurement of the proteasome's activity showed that trypsin-like activity was higher in *rox1*Δ than in the WT (Figure 4A). Conversely, chymotrypsin-like activity was significantly lower in *rox1*Δ than in the WT (Figure 4B). No significant difference in caspase-like activity was observed between the two strains (Figure 4C). When we examined the sensitivity to MG132 inhibition of the proteasome's activity, we observed no significant difference in sensitivity to the inhibition of trypsin-like or caspase-like activities between the *rox1*Δ and WT strains. However, the MG132 sensitivity of chymotrypsin-like activity in *rox1*Δ was suppressed compared with that in the WT (Figure 4B). Additionally, the cell viability of *rox1*Δ after freezing stress was higher than that of the WT (Figure 4D). Furthermore, the fermentation capacity of cells before and after freezing stress was measured. As shown in Figure 4E, there was no significant difference in fermentation capacity between *rox1*Δ and the WT before freezing stress. Intriguingly, after freezing stress, *rox1*Δ exhibited a higher fermentation capacity than the WT (Figure 4F). Therefore, deletion of *ROX1* may confer improved freezing tolerance in yeast.

Anb1 regulates the proteasome's activity and freezing stress tolerance by serving as a downstream effector of Rox1.

To our knowledge, there has been no report showing that Rox1 directly regulates the proteasome's activity. To clarify the downstream pathways of Rox1, we conducted a comprehensive transcriptional analysis (RNAseq analysis) before and after exposure to freezing stress. Since Rox1 is a transcriptional repressor, target genes would be upregulated in *rox1*Δ. We therefore searched for genes whose expression was upregulated more than two-fold in *rox1*Δ compared with the WT under all conditions before freezing and 20 or 40 min after thawing (Tables S3–S5). This process resulted in the extraction of 18 genes that met the criteria (Table S6 and Figure S3). There were no proteasome-related genes among

them, which may indicate that Rox1 indirectly regulates the proteasome's activity. Of the 18 candidate genes, 12 (*ANB1*, *YPR064W*, *HEM13*, *SUR2*, *DIA3*, *LAC1*, *ROG3*, *YPR015C*, *GID10*, *FRD1*, *MHF1*, and *YAR029W*) were available in the yeast ORF collection. By measuring the residual chymotrypsin-like activity in the presence of MG132 in the *erg6*Δ*pdr5*Δ strains overexpressing each candidate gene, we identified regulatory genes associated with the proteasome's activity. As observed above, the loss of the *ROX1* gene led to a reduction in the inhibition of chymotrypsin-like activity by MG132 (Figure 5A). More importantly, only the strain overexpressing *ANB1* exhibited decreased sensitivity of chymotrypsin-like activity to MG132. Anb1 functions as a translation elongation factor eIF-5A, aiding in the translation of proline-rich proteins. Next, we measured the proteasome's activity in the *ANB1*-overexpressing strain in the presence of absence of MG132. Trypsin-like activity was higher in the *ANB1*-overexpressing strain than in the parent strain, while chymotrypsin-like activity was lower (Figure 5B,C). There was no significant difference in caspase-like activity between the strains (Figure 5D). The MG132 sensitivity of trypsin-like and caspase-like activity was similar between the two strains (Figure 5B,D). On the other hand, the *ANB1*-overexpressing strain showed reduced MG132 sensitivity of chymotrypsin-like activity (Figure 5B). Furthermore, the *ANB1*-overexpressing strain exhibited much better tolerance to freezing stress than the parental strain (Figure 5E).

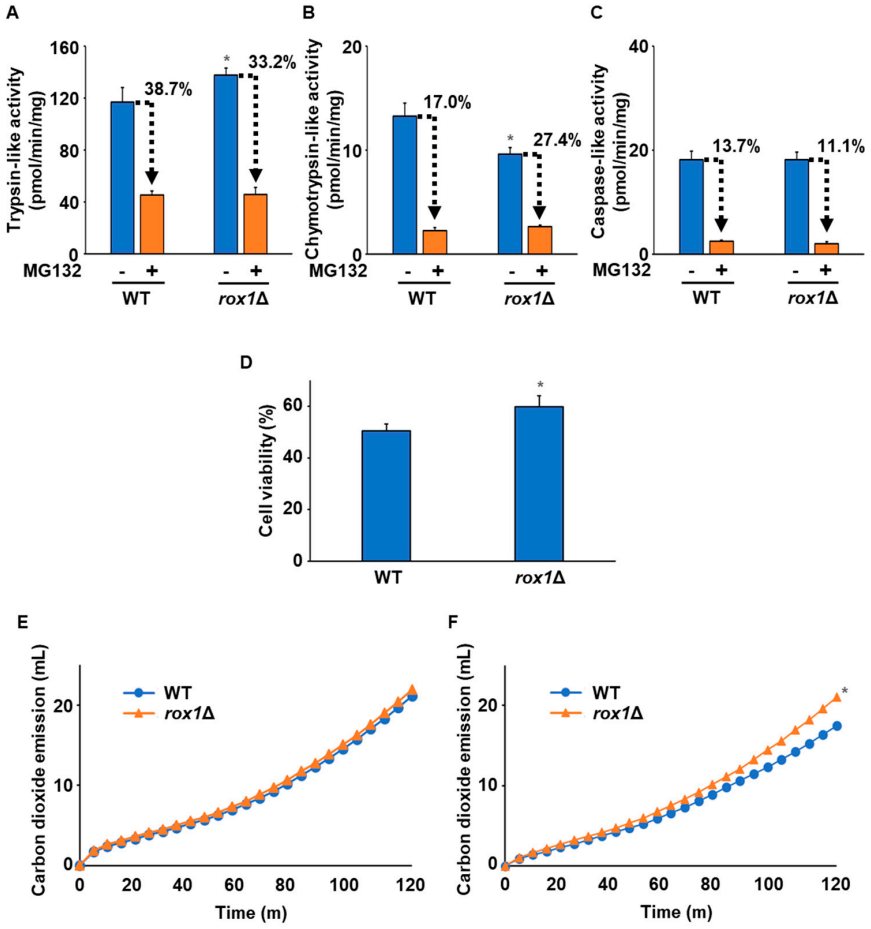


Figure 4. Characterization of the WT with deletion of *ROX1*. (**A**) Trypsin-like activity. Trypsin-like activity in the WT and *rox1*Δ strains was determined by the fluorescence of AMC generated from Ac-RLR-AMC during the enzymatic reaction without/with 50 μM MG132. Data are presented as the means ± SD (n = 3), and statistical significance was determined by Student's t-test. * $p < 0.05$ vs. WT -MG132. (**B**) Chymotrypsin-like activity. Chymotrypsin-like activity in the WT and *rox1*Δ strains was determined by the fluorescence of AMC generated from Suc-LLVY-MCA during the enzymatic reaction

without/with 50 μM MG132. Data are presented as the means ± SD (n = 3), and statistical significance was determined by Student's t-test. * $p < 0.05$ vs. WT -MG132. (**C**) Caspase-like activity. Caspase-like activity in the WT and *rox1*Δ strains was determined by the fluorescence of AMC generated from Z-LLE-MCA during the enzymatic reaction without/with 50 μM MG132. Data are presented as the means ± SD (n = 3), and statistical significance was determined by Student's t-test. (**D**) The cells' viability after freezing stress. The WT and *rox1*Δ strains were stored at −30 °C for 5 days. After thawing at 25 °C for 20 min, the cells were spread onto YPD plates, and the cells' viability was determined by measuring the colony-forming units. Data are presented as the means ± SD (n = 3), and statistical significance was determined by Student's t-test. * $p < 0.05$ vs. WT. (**E**) Model of the doughs' fermentation before freezing stress. The graph indicates the total carbon dioxide emission of the WT and *rox1*Δ strains before freezing stress. Three independent experiments were performed, but representative results are presented here due to the large variation in the absolute values. Statistical significance was determined by two-way analysis of variance with Tukey's test. (**F**) Model of the doughs' fermentation after freezing stress. The graph indicates the total carbon dioxide emission of the WT and *rox1*Δ strains after freezing stress (−30 °C, 5 days). Three independent experiments were performed, but representative results are presented here due to the large variation in the absolute values. Statistical significance was determined by two-way analysis of variance with Tukey's test. * $p < 0.05$ vs. WT.

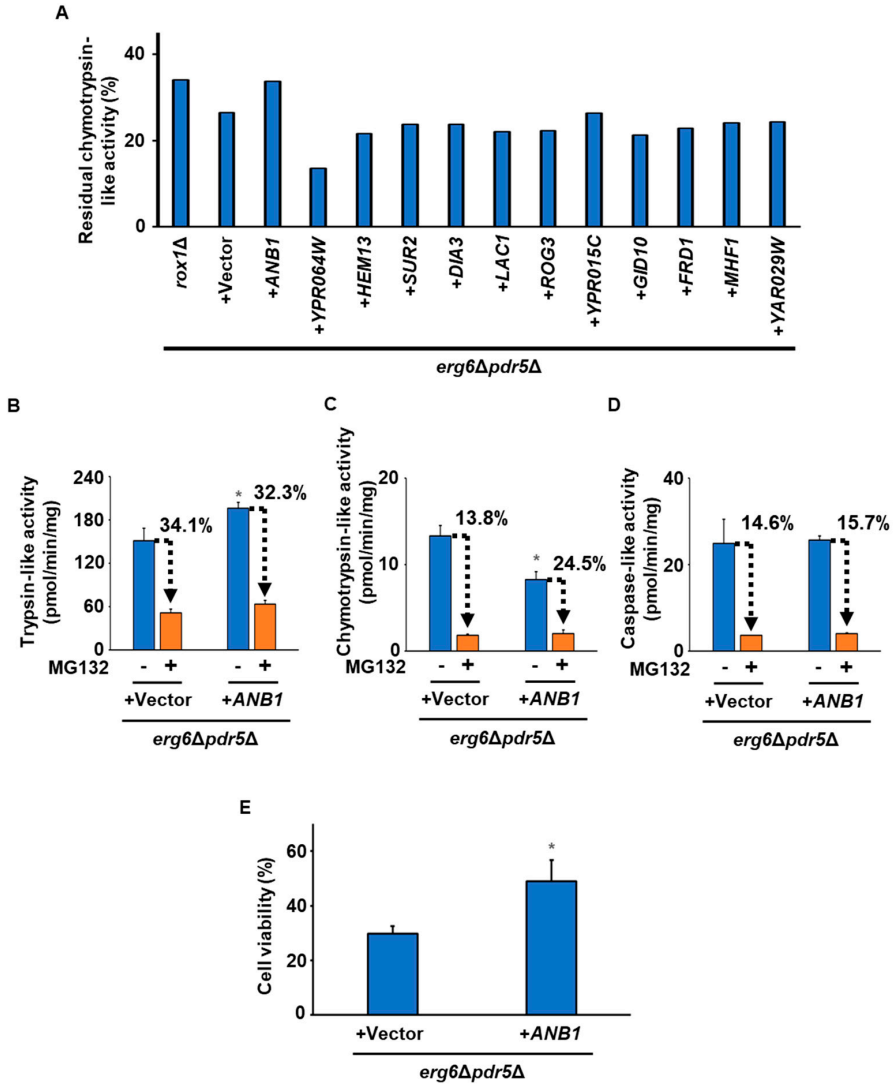


Figure 5. Screening of the genes responsible for regulating the proteasome's activity downstream from Rox1. (**A**) Residual chymotrypsin-like activity in the presence of MG132. Chymotrypsin-like activity in

*erg6*Δ*pdr5*Δ*rox1*Δ and *erg6*Δ*pdr5*Δ harboring pAG416-P_{GPD}-ccdB-HA (+vector), -ANB1 (+*ANB1*), -YPR064W (+*YPR064W*), -HEM13 (+*HEM13*), -SUR2 (+*SUR2*), -DIA3 (+*DIA3*), -LAC1 (+*LAC1*), -ROG3 (+*ROG3*), -YPR015C (+*YPR015C*), -GID10 (+*GID10*), -FRD1 (+*FRD1*), -MHF1 (+*MHF1*), or -YAR029W (+*YAR029W*) was determined by the fluorescence of AMC generated from Suc-LLVY-MCA during the enzymatic reaction with 50 μM MG132. The data represent a single experiment (n = 1). (**B**) Trypsin-like activity. Trypsin-like activity in *erg6*Δ*pdr5*Δ harboring pAG416-P_{GPD}-ccdB-HA (+vector) or pAG416-P_{GPD}-ANB1-HA (+*ANB1*) was determined by the fluorescence of AMC generated from Ac-RLR-AMC during the enzymatic reaction without/with 50 μM MG132. Data are presented as the means ± SD (n = 3), and statistical significance was determined by Student's t-test. * $p < 0.05$ vs. +vector -MG132. (**C**) Chymotrypsin-like activity. Chymotrypsin-like activity in *erg6*Δ*pdr5*Δ harboring pAG416-P_{GPD}-ccdB-HA (+vector) or pAG416-P_{GPD}-ANB1-HA (+*ANB1*) was determined by the fluorescence of AMC generated from Suc-LLVY-MCA during the enzymatic reaction without/with 50 μM MG132. Data are presented as the means ± SD (n = 3), and statistical significance was determined by Student's t-test. * $p < 0.05$ vs. +vector -MG132. (**D**) Caspase-like activity. Caspase-like activity in *erg6*Δ*pdr5*Δ harboring pAG416-P_{GPD}-ccdB-HA (+vector) or pAG416-P_{GPD}-ANB1-HA (+*ANB1*) was determined by the fluorescence of AMC generated from Z-LLE-MCA during the enzymatic reaction without/with 50 μM MG132. Data are presented as the means ± SD (n = 3), and statistical significance was determined by Student's t-test. (**E**) The cells' viability after freezing stress. The *erg6*Δ*pdr5*Δ strains harboring pAG416-P_{GPD}-ccdB-HA (+vector) or pAG416-P_{GPD}-ANB1-HA (+*ANB1*) were stored at −30 °C for 5 days. After thawing at 25 °C for 20 min, the cells were spread onto YPD plates, and the cells' viability was determined by measuring the colony-forming units. Data are presented as the means ± SD (n = 3), and statistical significance was determined by Student's t-test. * $p < 0.05$ vs. +vector.

Finally, we characterized the WT strain overexpressing *ANB1*. The *ANB1*-overexpressing strain had higher trypsin-like activity but lower chymotrypsin-like activity than the vector control (Figure 6A,B). Caspase-like activity did not differ between the two strains (Figure 6C). There was no significant difference between the two strains in sensitivity to MG132's inhibition of trypsin-like and caspase-like activities (Figure 6A,C). The *ANB1*-overexpressing strain showed decreased sensitivity to MG132 for chymotrypsin-like activity (Figure 6B). These results were consistent with those observed in the *ROX1*-deleting strain. We then measured the cells' viability after freezing stress. Figure 6D shows that *ANB1* deletion canceled the enhanced freezing stress tolerance of *rox1*Δ. The *ANB1* disruptant appeared to be less tolerant to freezing stress than the WT. As shown in Figure 6E, the strain overexpressing *ANB1* had higher tolerance to freezing stress than the vector control. Anb1 has a hypusinated lysine at Position 51, which is essential for the activity of eIF-5A. Significantly, overexpression of a variant of Anb1 (Anb1 K51R), in which the lysine at Position 51 was replaced with arginine, did not increase tolerance to freezing stress. Similarly, overproduction of *HYP2*, a paralog of *ANB1*, did not improve freezing stress tolerance. As shown in Figure 6F, there was no significant difference in fermentation ability between the vector control and the *ANB1*-overexpressing strain before freezing stress. More importantly, after freezing stress, the *ANB1*-overexpressing strain exhibited a higher fermentation performance than the vector control (Figure 6G). Thus, overexpression of Anb1 may alter the proteasome's activity, causing enhanced tolerance to freezing stress.

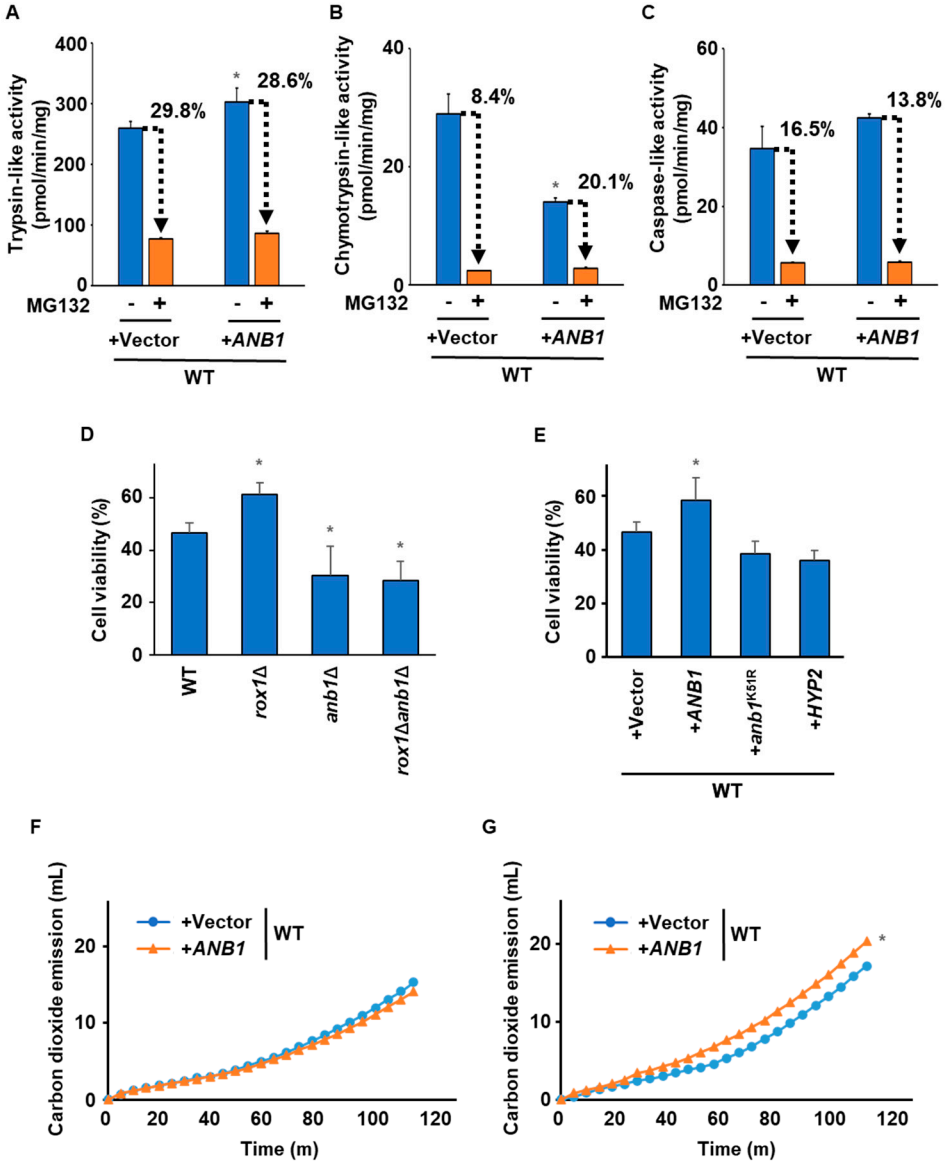


Figure 6. Effects of *ANB1* overexpression on the proteasome's activity and freezing stress tolerance. (**A**) Trypsin-like activity. Trypsin-like activity in the WT strains harboring pAG416-P_{GPD}-ccdB-HA (+vector) or pAG416-P_{GPD}-ANB1-HA (+*ANB1*) was determined by the fluorescence of AMC generated from Ac-RLR-AMC during the enzymatic reaction without/with 50 μM MG132. Data are presented as the means ± SD (n = 3), and statistical significance was determined by Student's t-test. * $p < 0.05$ vs. +vector -MG132. (**B**) Chymotrypsin-like activity. Chymotrypsin-like activity in the WT strains harboring pAG416-P_{GPD}-ccdB-HA (+vector) or pAG416-P_{GPD}-ANB1-HA (+*ANB1*) was determined by the fluorescence of AMC generated from Suc-LLVY-MCA during the enzymatic reaction without/with 50 μM MG132. Data are presented as the means ± SD (n = 3), and statistical significance was determined by Student's t-test. * $p < 0.05$ vs. +vector -MG132. (**C**) Caspase-like activity. Caspase-like activity in the WT strains harboring pAG416-P_{GPD}-ccdB-HA (+Vector) or pAG416-P_{GPD}-ANB1-HA (+*ANB1*) was determined by the fluorescence of AMC generated from Z-LLE-MCA during the enzymatic reaction without/with 50 μM MG132. Data are presented as the means ± SD (n = 3), and statistical significance was determined by Student's t-test. (**D**) The cells' viability after freezing stress. WT, *rox1*Δ, *anb1*Δ, and *rox1*Δ*anb1*Δ were stored at −30 °C for 5 days. After thawing at 25 °C for 20 min, the cells were spread onto YPD plates, and the cells' viability was determined by measuring the colony-forming units. Data are presented as the means ± SD (n = 3),

and statistical significance was determined by Student's *t*-test. * $p < 0.05$ vs. WT. (**E**) The cells' viability after freezing stress. The WT strains harboring pAG416-P_{GPD}-ccdB-HA (+vector), pAG416-P_{GPD}-ANB1-HA (+*ANB1*), pAG416-P_{GPD}-anb1^{K51R}-HA (+*anb1*^{K51R}), or pAG416-P_{GPD}-HYP2-HA (+*HYP2*) were stored at −30 °C for 5 days. After thawing at 25 °C for 20 min, the cells were spread onto YPD plates, and the cells' viability was determined by measuring the colony-forming units. Data are presented as the means ± SD ($n = 3$), and statistical significance was determined by Student's *t*-test. * $p < 0.05$ vs. +vector. (**F**) Model of the doughs' fermentation before freezing stress. The graph indicates the total carbon dioxide emissions of the WT strains harboring pAG416-P_{GPD}-ccdB-HA (+vector) or pAG416-P_{GPD}-ANB1-HA (+*ANB1*) before freezing stress. Three independent experiments were performed, but representative results are presented here due to the large variation in the absolute values. Statistical significance was determined by two-way analysis of variance with Tukey's test. (**G**) Model of the doughs' fermentation after freezing stress. The graph indicates the total carbon dioxide emissions of the WT strains harboring pAG416-P_{GPD}-ccdB-HA (+vector) or pAG416-P_{GPD}-ANB1-HA (+*ANB1*) after freezing stress (−30 °C, 5 days). Three independent experiments were performed, but representative results are presented here due to the large variation in the absolute values. Statistical significance was determined by two-way analysis of variance with Tukey's test. * $p < 0.05$ vs. +vector.

4. Discussion

Frozen dough baking is a promising technology for future advancements in food manufacturing technology. This process can lead to intense freezing stress on yeast cells, which reduces the bread's quality. In a previous study, Watanabe et al. found that the expression level of proteasome-related genes was reduced, and ubiquitinated proteins were accumulated by freeze–thaw stress in strains with reduced fermentation ability after cryopreservation [8]. These results suggested that the proteasome's function is involved in fermentation ability after freezing stress. Expanding upon their findings, our present results indicated that the Rox1–Anb1 pathway represses freezing stress tolerance by altering the proteasome's activity. Moreover, deletion of *ROX1* or overexpression of *ANB1* improved the fermentation performance after exposure to the stress. These findings provide insight into the mechanisms of tolerance to freezing stress and their potential applications in the development of baker's yeast strains.

Anb1 and Hyp2 (encoded by the *ANB1* paralog gene) are isoforms of the translation elongation factor eIF-5A, which supports the synthesis of nascent proline-rich proteins by mitigating translational stalling [32]. Anb1 and Hyp2 share over 90% similarity in their amino acid sequences, suggesting that they recognize the same proteins. However, when overexpressed, Anb1 and Hyp2 have different effects on freezing stress tolerance, suggesting that they have distinct substrate specificities. To better understand these differences, we need to investigate the expression of proline-rich proteins in the *ROX1*-deleted and *ANB1*-overexpressing strains. This will help us determine the precise substrate specificities of Anb1 and Hyp2.

Among the proteasome-related proteins, Pre2 and Fub1 have proline-rich motifs. The N-terminal site of Pre2, which has chymotrypsin-like activity, is known as a molecular chaperone (β5pro) that promotes the 26S proteasome's association, thereby stabilizing the 26S proteasome [33]. Thus, enhanced translation of Pre2 in the *ROX1*-disrupted and *ANB1*-overexpressing strains might lead to improved clearance of denatured proteins by the proteasome. However, the elevated expression of Pre2 may correspondingly result in increased chymotrypsin-like activity, which could contradict the findings presented in this study. Fub1, an ortholog of mammalian PI31, is an intrinsic inhibitor of the proteasome's activity in vitro [34,35]. The structural analysis revealed that the homodimer of Fub1 binds to the catalytic pocket (β1: caspase-like enzyme Pre3; β2: trypsin-like enzyme Pup1; β5: chymotrypsin-like enzyme Pre2) of the 26S proteasome. Notably, Fub1 may bind near β5, inhibiting chymotrypsin-like activity while exerting little effect on the caspase-like activity of β1, which is sterically distant from β5 [36]. In addition, Fub1 forms hydrogen bonds with

the amino acid residues within β2, suggesting that these bonds may affect the trypsin-like activity of β2. Thus, overtranslation of Fub1 might contribute to changes in the proteasome's activity, as observed in the *rox1*Δ and *ANB1*-overexpressing strains. Peptide-based proteasome inhibitors such as MG132 are known to bind to the catalytic pocket of the 26S proteasome [18]. Therefore, Fub1 and MG132 could bind competitively. The resistance of the *ROX1*-disrupted strain to MG132 might be attributed to the pre-existing Fub1 at the catalytic pocket. Previous reports have suggested that Fub1 inhibits the proteasome's activity in vitro but assists in stabilizing the proteasome's conformation and degrading substrate proteins in vivo [37]. Freezing and thawing are complex stresses, including the formation of ice crystals, ROS generation, and dehydration. The proteasome is reportedly vulnerable to oxidative damage, which occurs under freezing stress conditions, and ROS can disrupt the proteasome's structure [38]. Therefore, Fub1 may stabilize the proteasome's structure under freezing stress conditions by binding to the proteasome. The Fub1-bound proteasome may also facilitate the recruitment of substrate proteins and efficiently degrade the denatured proteins generated during freezing stress. Under the low-oxygen conditions where the expression of *ANB1* is induced due to the release of Rox1 inhibition, mitochondrial ROS production is increased [39]. Rox1 is hypothesized to induce the expression of *ANB1* in response to low oxygen, thereby protecting the proteasome from oxidative damage. Additionally, the Fub1-bound proteasome may facilitate the recruitment of substrate proteins, potentially enabling the efficient degradation of denatured proteins arising from freezing stress. The mechanism underlying freezing stress tolerance in the Rox1–Anb1 pathway may be clarified through observations of the proteasome's structure and identification of the denatured proteins that accumulate under freezing stress conditions.

Since proteasome inhibitors such as MG132 cannot penetrate yeast cells' membranes, it is quite hard to show sensitivity or resistance to proteasome inhibitors. In this study, MG132-sensitive yeast strains were constructed using genetic recombination technology. The use of genetic engineering techniques for breeding yeast is challenging due to consumer and public concerns regarding its safety. Here, we have the possibility that treatment with low concentrations of amphotericin, which binds to ergosterol, may increase the permeability of proteasome inhibitors into yeast cells, leading to increased sensitivity to them. We plan to investigate this screening method in practical baker's yeast in the future. Additionally, this breeding method could be applied to creating yeast strains with enhanced tolerance to stresses other than freezing because the proteasome is crucial for many stresses that induce protein denaturation. In fermentation environments other than bread making, there are various factors that induce stress conditions, such as high ethanol concentrations, high osmotic pressure, low or high temperatures, and oxidation, all of which can denature intracellular proteins. Hence, this breeding strategy has the potential to be utilized in the construction of various practical yeast strains beyond baker's yeast.

5. Conclusions

In this study, we investigated the relationship between the ubiquitin–proteasome system and freezing stress tolerance in *S. cerevisiae*. Screening with MG132 isolated some mutants with enhanced freezing stress tolerance, characterized by increased intracellular activity of the proteasome, particularly the proteasome's trypsin-like activity, and by decreased sensitivity to MG132's inhibition of chymotrypsin-like activity. Whole-genome sequencing showed that loss-of-function mutations in *ROX1*, a heme-dependent repressor of hypoxic genes, result in enhanced freezing stress tolerance. Therefore, transcription analysis revealed *ANB1* as a potential downstream target gene of Rox1. This study proposes a new mechanism for enhancing stress tolerance during freezing mediated by the ubiquitin–proteasome system. By applying the knowledge gained from this study to the development of baker's yeast strains, we can improve the baking process of frozen dough to produce higher-quality bread. Furthermore, elucidation of the regulatory mechanism underlying the ubiquitin–proteasome system is expected to provide valuable insights into quality control mechanisms of protein.

Supplementary Materials: The following supporting information can be downloaded at https://www.mdpi.com/article/10.3390/fermentation10060318/s1. Table S1: Yeast strains used in this study. Table S2: Oligonucleotide primers used in this study. Table S3: List of genes whose expression was increased more than twofold in rox1Δ compared with the WT before being frozen. Table S4: List of genes whose expression was increased more than twofold in rox1Δ compared with the WT at 20 min after thawing. Table S5: List of genes whose expression was increased more than twofold in rox1Δ compared with the WT at 40 min after thawing. Table S6: List of genes whose expression was increased more than twofold in rox1Δ compared with the WT in all conditions: before freezing and at 20 or 40 min after thawing. Figure S1: Negative effects of freezing stress on the cell viability and fermentation ability. Figure S2: Characterization of the *rpn4*Δ and *ubr2*Δ strains. Figure S3: Venn diagram representing the number of upregulated genes in *rox1*Δ.

Author Contributions: Conceptualization, A.N.; methodology, A.N., K.K., N.I., S.F. and H.E.; software, none; validation, R.T., A.N., K.K., N.I., S.F. and H.E.; formal analysis, R.T. and A.N.; investigation, A.N. and K.K.; resources, A.N., K.K., N.I., S.F. and H.E.; data curation, A.N. and K.K.; writing—original draft preparation, R.T.; writing—review and editing, A.N. and H.T.; visualization, R.T. and K.K.; supervision, A.N. and H.T.; project administration, A.N. and H.T.; funding acquisition, R.T., A.N. and H.T. All authors have read and agreed to the published version of the manuscript.

Funding: This research was partly supported by a Grant-in-Aid for Early-Career Scientists (23K13872) to R.T., a Grant-in-Aid for Scientific Research (C) (21K05504) to A.N., and a Grant-in-Aid for Scientific Research (S) (19H05639) to H.T.

Data Availability Statement: Whole-genome sequences and RNAseq data supporting the findings of this study are available in the DDBJ Sequenced Read Archive under the accession numbers DRR352989, DRR352990, DRR352991, DRR352992, DRR352993, DRR425985, DRR425986, DRR425987, DRR425988, DRR425989, and DRR425990.

Acknowledgments: We would like to thank Chie Murayama for her technical support.

Conflicts of Interest: Authors Natsumi Ishizaki, Shiho Fujishima and Hisanori Endo were employed by the company Food R&D Center, TableMark Co., Ltd. The remaining authors declare that the research was conducted in the absence of any commercial or financial relationships that could be construed as a potential conflict of interest.

References

1. George, R.M. Freezing processes used in the food industry. *Trends Food Sci. Technol.* **1993**, *4*, 134–138. [CrossRef]
2. Ribotta, P.D.; León, A.E.; Añón, M.C. Effects of yeast freezing in frozen dough. *Cereal Chem.* **2003**, *80*, 454–458. [CrossRef]
3. Naicker, M.C.; Seul Jo, I.; Im, H. Identification of chaperones in freeze tolerance in *Saccharomyces cerevisiae*. *J. Microbiol.* **2012**, *50*, 882–887. [CrossRef] [PubMed]
4. Sasano, Y.; Haitani, Y.; Hashida, K.; Ohtsu, I.; Shima, J.; Takagi, H. Simultaneous accumulation of proline and trehalose in industrial baker's yeast enhances fermentation ability in frozen dough. *J. Biosci. Bioeng.* **2012**, *113*, 592–595. [CrossRef]
5. Cabrera, E.; Welch, L.C.; Robinson, M.R.; Sturgeon, C.M.; Crow, M.M.; Segarra, V.A. Cryopreservation and the freeze–thaw stress response in yeast. *Genes* **2020**, *11*, 835. [CrossRef]
6. Attfield, P.V. Stress tolerance: The key to effective strains of industrial baker's yeast. *Nat. Biotechnol.* **1997**, *15*, 1351–1357. [CrossRef] [PubMed]
7. Shima, J.; Sakata-Tsuda, Y.; Suzuki, Y.; Nakajima, R.; Watanabe, H.; Kawamoto, S.; Takano, H. Disruption of the *CAR1* gene encoding arginase enhances freeze tolerance of the commercial baker's yeast *Saccharomyces cerevisiae*. *Appl. Environ. Microbiol.* **2003**, *69*, 715–718. [CrossRef]
8. Watanabe, D.; Sekiguchi, H.; Sugimoto, Y.; Nagasawa, A.; Kida, N.; Takagi, H. Importance of proteasome gene expression during model dough fermentation after preservation of baker's yeast cells by freezing. *Appl. Environ. Microbiol.* **2018**, *84*, e00406-18. [CrossRef]
9. Hochstrasser, M. Ubiquitin-dependent protein degradation. *Annu. Rev. Genet.* **1996**, *30*, 405–439. [CrossRef]
10. Hershko, A.; Ciechanover, A. The ubiquitin system. *Annu. Rev. Biochem.* **1998**, *67*, 425–479. [CrossRef]
11. Marshall, R.S.; Vierstra, R.D. Dynamic regulation of the 26S proteasome: From synthesis to degradation. *Front. Mol. Biosci.* **2019**, *6*, 40. [CrossRef]
12. Bhattacharyya, S.; Yu, H.; Mim, C.; Matouschek, A. Regulated protein turnover: Snapshots of the proteasome in action. *Nat. Rev. Mol. Cell. Biol.* **2014**, *15*, 122–133. [CrossRef] [PubMed]
13. Finley, D. Recognition and processing of ubiquitin-protein conjugates by the proteasome. *Annu. Rev. Biochem.* **2009**, *78*, 477–513. [CrossRef] [PubMed]

14. Matyskiela, M.E.; Martin, A. Design principles of a universal protein degradation machine. *J. Mol. Biol.* **2013**, *425*, 199–213. [CrossRef] [PubMed]
15. Deveraux, Q.; Ustrell, V.; Pickart, C.; Rechsteiner, M. A 26 S protease subunit that binds ubiquitin conjugates. *J. Biol. Chem.* **1994**, *269*, 7059–7061. [CrossRef] [PubMed]
16. Husnjak, K.; Elsasser, S.; Zhang, N.; Chen, X.; Randles, L.; Shi, Y.; Hofmann, K.; Walters, K.J.; Finley, D.; Dikic, I. Proteasome subunit Rpn13 is a novel ubiquitin receptor. *Nature* **2008**, *453*, 481–488. [CrossRef] [PubMed]
17. Thrower, J.S.; Hoffman, L.; Rechsteiner, M.; Pickart, C.M. Recognition of the polyubiquitin proteolytic signal. *EMBO J.* **2000**, *19*, 94–102. [CrossRef] [PubMed]
18. Guo, N.; Peng, Z. MG132, a proteasome inhibitor, induces apoptosis in tumor cells. *Asia Pac. J. Clin. Oncol.* **2013**, *9*, 6–11. [CrossRef] [PubMed]
19. Mannhaupt, G.; Schnall, R.; Karpov, V.; Vetter, I.; Feldmann, H. Rpn4p acts as a transcription factor by binding to PACE, a nonamer box found upstream of 26S proteasomal and other genes in yeast. *FEBS Lett.* **1999**, *450*, 27–34. [CrossRef]
20. Xie, Y.; Varshavsky, A. RPN4 is a ligand, substrate, and transcriptional regulator of the 26S proteasome: A negative feedback circuit. *Proc. Natl. Acad. Sci. USA* **2001**, *98*, 3056–3061. [CrossRef]
21. Wang, L.; Mao, X.; Ju, D.; Xie, Y. Rpn4 is a physiological substrate of the Ubr2 ubiquitin ligase. *J. Biol. Chem.* **2004**, *279*, 55218–55223. [CrossRef]
22. Kusmierczyk, A.R.; Hochstrasser, M. Some assembly required: Dedicated chaperones in eukaryotic proteasome biogenesis. *Biol. Chem.* **2008**, *389*, 1143–1151. [CrossRef] [PubMed]
23. Murata, S.; Yashiroda, H.; Tanaka, K. Molecular mechanisms of proteasome assembly. *Nat. Rev. Mol.* **2009**, *10*, 104–115. [CrossRef] [PubMed]
24. Matias, A.C.; Ramos, P.C.; Dohmen, R.J. Chaperone-assisted assembly of the proteasome core particle. *Biochem. Soc. Trans.* **2010**, *38*, 29–33. [CrossRef] [PubMed]
25. Chen, P.; Hochstrasser, M. Autocatalytic subunit processing couples active site formation in the 20S proteasome to completion of assembly. *Cell* **1996**, *86*, 961–972. [CrossRef] [PubMed]
26. Jäger, S.; Groll, M.; Huber, R.; Wolf, D.H.; Heinemeyer, W. Proteasome beta-type subunits: Unequal roles of propeptides in core particle maturation and a hierarchy of active site function. *J. Mol. Biol.* **1999**, *291*, 997–1013. [CrossRef] [PubMed]
27. Li, X.; Kusmierczyk, A.R.; Wong, P.; Emili, A.; Hochstrasser, M. beta-Subunit appendages promote 20S proteasome assembly by overcoming an Ump1-dependent checkpoint. *EMBO J.* **2007**, *26*, 2339–2349. [CrossRef] [PubMed]
28. Kruegel, U.; Robison, B.; Dange, T.; Kahlert, G.; Delaney, J.R.; Kotireddy, S.; Tsuchiya, M.; Tsuchiyama, S.; Murakami, C.J.; Schleit, J.; et al. Elevated proteasome capacity extends replicative lifespan in *Saccharomyces cerevisiae*. *PLoS Genet.* **2011**, *7*, e1002253. [CrossRef] [PubMed]
29. Simon, J.A. Yeast as a model system for anticancer drug discovery. *Expert. Opin. Ther Targets* **2001**, *5*, 177–195. [CrossRef]
30. Rahman, H.; Carneglia, J.; Lausten, M.; Robertello, M.; Choy, J.S.; Golin, J. Robust, pleiotropic drug tolerance 5 (Pdr5)-mediated multidrug tolerance is vigorously maintained in *Saccharomyces cerevisiae* cells during glucose and nitrogen limitation. *FEMS Yeast Res.* **2018**, *18*, foy029. [CrossRef]
31. Kwast, K.E.; Burke, P.V.; Poyton, R.O. Oxygen sensing and the transcriptional regulation of oxygen-responsive genes in yeast. *J. Exp. Biol.* **1998**, *201*, 1177–1195. [CrossRef] [PubMed]
32. Gregio, A.P.; Cano, V.P.; Avaca, J.S.; Valentini, S.R.; Zanelli, C.F. eIF5A has a function in the elongation step of translation in yeast. *Biochem. Biophys. Res. Commun.* **2009**, *380*, 785–790. [CrossRef] [PubMed]
33. Li, X.; Li, Y.; Arendt, C.S.; Hochstrasser, M. Distinct elements in the proteasomal β5 subunit propeptide eequired for autocatalytic processing and proteasome assembly. *J. Biol. Chem.* **2016**, *291*, 1991–2003. [CrossRef] [PubMed]
34. Zaiss, D.M.; Standera, S.; Holzhütter, H.; Kloetzel, P.; Sijts, A.J. The proteasome inhibitor PI31 competes with PA28 for binding to 20S proteasomes. *FEBS Lett.* **1999**, *457*, 333–338. [CrossRef] [PubMed]
35. McCutchen-Maloney, S.L.; Matsuda, K.; Shimbara, N.; Binns, D.D.; Tanaka, K.; Slaughter, C.A.; DeMartino, G.N. cDNA cloning, expression, and functional characterization of PI31, a proline-rich inhibitor of the proteasome. *J. Biol. Chem.* **2000**, *275*, 18557–18565. [CrossRef] [PubMed]
36. Rawson, S.; Walsh, R.M., Jr.; Velez, B.; Schnell, H.M.; Jiao, F.; Blickling, M.; Ang, J.; Bhanu, M.K.; Huang, L.; Hanna, J. Yeast PI31 inhibits the proteasome by a direct multisite mechanism. *Nat. Struct. Mol. Biol.* **2022**, *29*, 791–800. [CrossRef]
37. Yashiroda, H.; Toda, Y.; Otsu, S.; Takagi, K.; Mizushima, T.; Murata, S. N-terminal α7 deletion of the proteasome 20S core particle substitutes for yeast PI31 function. *Mol. Cell. Biol.* **2015**, *35*, 141–152. [CrossRef]
38. Wang, X.; Yen, J.; Kaiser, P.; Huang, L. Regulation of the 26S proteasome complex during oxidative stress. *Sci. Signal.* **2010**, *3*, ra88. [CrossRef] [PubMed]
39. Chandel, N.S.; Maltepe, E.; Goldwasser, E.; Mathieu, C.E.; Simon, M.C.; Schumacker, P.T. Mitochondrial reactive oxygen species trigger hypoxia-induced transcription. *Proc. Natl. Acad Sci. USA* **1998**, *95*, 11715–11720. [CrossRef]

Disclaimer/Publisher's Note: The statements, opinions and data contained in all publications are solely those of the individual author(s) and contributor(s) and not of MDPI and/or the editor(s). MDPI and/or the editor(s) disclaim responsibility for any injury to people or property resulting from any ideas, methods, instructions or products referred to in the content.